Articles

Interaction of Pyridine Nucleotide Substrates with *Escherichia coli* Dihydrodipicolinate Reductase: Thermodynamic and Structural Analysis of Binary Complexes[†,‡]

Sreelatha G. Reddy,[§] Giovanna Scapin,[§] and John S. Blanchard*

Department of Biochemistry, Albert Einstein College of Medicine, 1300 Morris Park Avenue, Bronx, New York 10461

Received July 1, 1996; Revised Manuscript Received August 8, 1996[⊗]

ABSTRACT: *E. coli* dihydrodipicolinate reductase exhibits unusual nucleotide specificity, with NADH being kinetically twice as effective as NADPH as a reductant as evidenced by their relative *V/K* values. To investigate the nature of the interactions which determine this specificity, we performed isothermal titration calorimetry to determine the thermodynamic parameters of binding and determined the three-dimensional structures of the corresponding enzyme−nucleotide complexes. The thermodynamic binding parameters for NADPH and NADH were determined to be $K_d = 2.12\ \mu$M, $\Delta G° = -7.81$ kcal mol^{-1}, $\Delta H° = -10.98$ kcal mol^{-1}, and $\Delta S° = -10.5$ cal mol^{-1} deg^{-1} and $K_d = 0.46\ \mu$M, $\Delta G° = -8.74$ kcal mol^{-1}, $\Delta H° = -8.93$ kcal mol^{-1}, and $\Delta S° = 0.65$ cal mol^{-1} deg^{-1}, respectively. The structures of DHPR complexed with these nucleotides have been determined at 2.2 Å resolution. The 2′-phosphate of NADPH interacts electrostatically with Arg39, while in the NADH complex this interaction is replaced by hydrogen bonds between the 2′ and 3′ adenosyl ribose hydroxyls and Glu38. Similar studies were also performed with other pyridine nucleotide substrate analogs to determine the contributions of individual groups on the nucleotide to the binding affinity and enthalpic and entropic components of the free energy of binding, $\Delta G°$. Analogs lacking the 2′-phosphate group bound with a 4−5-fold higher affinity to the protein compared to their 2′-phosphate containing homologs. For all analogs, the total binding free energy can be shown to include compensating enthalpic and entropic contributions to the association constants. The entropy contribution appears to play a more important role in the binding of the nonphosphorylated analogs than in the binding of the phosphorylated analogs.

Dihydrodipicolinate reductase (DHPR), encoded by the *dap*B gene, catalyzes the pyridine nucleotide-dependent reduction of dihydrodipicolinic acid (DHP) to form tetrahydrodipicolinic acid (THP; Scheme 1). The enzyme is a component of the biosynthetic pathway leading to *meso*-diaminopimelic acid (DAP) and L-lysine in bacteria. DAP is a component of the peptidoglycan layer of Gram-negative bacterial cell walls, and inhibition of its biosynthesis results in cell death, probably due to the instability of the peptidoglycan (Cirillo et al., 1994). L-Lysine is produced by the subsequent enzymatic decarboxylation of DAP and is essential for protein synthesis. This suggests that DHPR is a target for the design of inhibitors which may exhibit antibiotic activity.

Escherichia coli DHPR exhibits unusual pyridine nucleotide specificity, with NADH being bound more tightly ($K_d = 0.46\ \mu$M) than NADPH ($K_d = 2.1\ \mu$M) and with a wide variety of pyridine nucleotides being effective substrates (Reddy et al., 1995). Pyridine nucleotide-dependent enzymes typically show a substantial preference for one of the two nucleotides, and in other dual specificity enzymes studied, the steady-state K_m values of NADH are an order of magnitude higher than the equivalent values for NADPH[1] (Male & Storey, 1982; John et al., 1994). The cofactor specificity may be opposite for enzymes isolated from different sources: the *Clostridium symbiosum* glutamate dehydrogenase uses only NADH, while the *E. coli* enzyme

Scheme 1: Reaction Catalyzed by *E. coli* Dihydrodipicolinate Reductase

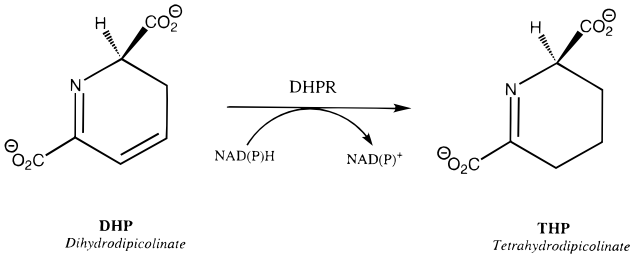

DHP *Dihydrodipicolinate* **THP** *Tetrahydrodipicolinate*

[†] This work was supported by NIH Grant AI33696.

[‡] Coordinates have been deposited with the Brookhaven Protein Data Bank. PDB codes for the DHPR−NADH, DHPR−3-Ac-NADH, and DHPR−NHDH complexes are 1DRU, 1DRV, and 1DRW, respectively.

* Author to whom correspondence should be addressed. Phone: (718) 430-3096. FAX: (718) 430-8565.

[§] Both authors contributed equally to this work.

[⊗] Abstract published in *Advance ACS Abstracts,* October 1, 1996.

[1] Abbreviations: Hepes, 2-(2-hydroxyethyl)-1-piperazineethanesulfonic acid; β-NAD(P)H, reduced β-nicotinamide adenine dinucleotide 2′-phosphate; TNAD(P)H, reduced β-thionicotinamide adenine dinucleotide 2′-phosphate; NHD(P)H, reduced β-nicotinamide hypoxanthine dinucleotide 2′-phosphate; 3′-NADPH, reduced β-nicotinamide adenine dinucleotide 3′-phosphate; 3-Ac-NADH, reduced β-3-acetylpyridine adenine dinucleotide; RMS, root mean square.

S0006-2960(96)01580-2 CCC: $12.00

is strictly NADPH dependent (Baker et al., 1992a). Enzymes that have been characterized as exhibiting dual nucleotide specificity include bovine liver glutamate dehydrogenase (Male & Storey, 1982), glyceraldehyde-3-phosphate dehydrogenase from maize chloroplast (Quigley et al., 1989), and glucose-6-phosphate dehydrogenase from *Leuconostoc mesenteroides* (DeMoss et al., 1953). A number of studies based on primary sequence comparisons, and when available on three-dimensional structures, have attempted to explain the molecular basis for the specificity exhibited by an enzyme for one cofactor over the other. Several studies have focused on the fingerprint region of the nucleotide binding fold (the $\beta\alpha\beta$-fold, containing the conserved GXGXXG or GXXGXXG sequence and an acidic residue 20−30 residues downstream of the glycine-rich region at the C-terminus of the second β-strand) in order to identify patterns or residues that would predict the nucleotide selectivity. These studies have failed to produce a general rule which can successfully be used in a predictive fashion (Scrutton et al., 1990; Baker et al., 1992a). Baker et al. have suggested that the coenzyme specificity of NAD^+-dependent dehydrogenases is based on hydrogen-bonding interactions between the main chain amide nitrogen of the second residue of the consensus sequence and the "conserved acidic residue", which is involved in hydrogen-bonding interactions with the O2′ and O3′ hydroxyls of the adenosyl ribose ring. However, this acidic residue is often present in both dual specificity and NADPH-dependent enzymes. Baker et al. (1992b) have proposed that a favorable interaction between enzymes and NADH may depend on the size of the O2′ binding cavity. A number of studies have correlated NADPH selectivity to the presence of conserved basic residues, particularly arginine residues, near the C-terminal portion of the second β-strand of the $\beta\alpha\beta$-fold. These residues provide stabilizing eletrostatic interactions for the negative charge carried by the 2′-phosphate (Bystroff et al., 1990; Scrutton et al., 1990; Sem & Kasper, 1993). In the X-ray crystallographically determined three-dimensional structure of the glutathione reductase−NADPH complex, the total number and length of hydrogen bonds made in the enzyme−NADPH complex play a role in defining the overall energy of the binding and the high specificity for NADPH (Karplus & Schulz, 1989).

The present study was undertaken to investigate the thermodynamics of binding of pyridine nucleotide substrates to *E. coli* DHPR, an enzyme which intrinsically exhibits only modest discrimination between 2′-phosphorylated and nonphosphorylated pyridine nucleotide substrates and exhibits broad pyridine nucleotide specificity (Reddy et al., 1995). The *E. coli* dihydrodipicolinate reductase is an ideal subject for this investigation since the recombinant enzyme (rDHPR) is available in large quantities, and its three-dimensional structure has been determined at high resolution using X-ray crystallography (Scapin et al., 1995). The thermodynamic parameters for nucleotide binding, determined by isothermal titration microcalorimetry, have provided information on the relative enthalpic and entropic contributions to the free energy of nucleotide binding. The determination of the three-dimensional structures of the *E. coli* DHPR−NADPH and DHPR−NADH complexes allows us to perform a detailed analysis of the mode of binding for phosphorylated and nonphosphorylated nucleotides. In addition, the structures of two other binary enzyme−nucleotide complexes with nucleotide substrates modified in the carboxamido side chain (DHPR−3-acetyl-NADH), and in the adenine moiety (DHPR−NHDH), provide additional information on nucleotide binding interactions with *E. coli* DHPR.

MATERIALS AND METHODS

Glutathione reductase from yeast, NADH peroxidase from *Streptococcus faecalis*, all pyridine nucleotides, and buffer components were purchased from Sigma. Recombinant dihydrodipicolinate reductase was purified from *E. coli* and assayed as described previously (Reddy et al., 1995). The concentrations of the phosphorylated and nonphosphorylated pyridine nucleotide analogs were determined by enzymatic end-point assays with glutathione reductase and NADH peroxidase, respectively.

Isothermal Titration Microcalorimetry. Nucleotide binding to *E. coli* DHPR was analyzed in a Microcal Omega titration calorimeter from Microcal, Inc. (Northampton, MA), temperature equilibrated at 28 °C. The instrument and the equations used to fit calorimetric data have been described in detail previously (Wiseman et al., 1989). Purified DHPR was exchanged into 20 mM Hepes/KOH, pH 7.8, by gel filtration chromatography on a 1.6 × 60 cm Superdex 200 (Pharmacia) column. The enzyme concentration was determined using a dye-binding assay (Bradford, 1976). Nucleotide solutions were prepared in the same buffer, and enzyme and nucleotide solutions were thoroughly degassed by gentle stirring under vacuum. In a typical experiment, the 1.36 mL sample cell was filled with an 80 μM solution of DHPR. To this solution were added 4.0 μL injections, from a 100 μL syringe rotating at 350 rpm, of 1−2 mM solutions of nucleotide. Typically, 25 injections of 8 s duration were made at 4 min intervals. The heats of reaction were determined by integration of the peak obtained. To correct for the nucleotide heat of dilution, control experiments were performed under identical conditions with the sample cell containing buffer alone. After the contribution from the heat of dilution of each injection was subtracted, the sum of the heat evolved was plotted against the total ligand concentration to produce the binding isotherm. Binding constants, K_a, enthalpies of binding, $\Delta H°$, and stoichiometry, n, were determined by fitting the binding isotherm to the equation described previously (Wiseman et al., 1989) for ligand binding to a macromolecule possessing one set of independent ligand binding sites. The data were deconvoluted using a nonlinear least-squares algorithm incorporated in the Origin software provided with the instrument (Wiseman et al., 1989). The fitting process requires that initial estimates of n, K_a, and $\Delta H°$ be provided, and iteration proceeds until no further improvement in the calculated and observed data is achieved. The errors reported in n, K_a, and $\Delta H°$ are generated by the Origin program and reflect the quality of the fit between the nonlinear least-squares curve and the experimental points in Figure 1. $\Delta G°$ values were calculated from K_a values ($\Delta G° = -RT \ln K_a$), and $\Delta S°$ values were calculated from $\Delta G°$ and $\Delta H°$ values [$\Delta S° = (\Delta G° - \Delta H°)/T$]. Errors reported in Table 3 for $\Delta G°$ and $\Delta S°$ were propagated from the errors of K_a and $\Delta H°$, repectively. The ratios of the observed K_d's for NADPH and NADH agreed well with those from previous reported kinetic constants.

Crystallization. Crystals of *E. coli* DHPR complexed with NADPH, NADH, NHDH, and 3-Ac-NADH were prepared by the hanging drop vapor diffusion method as described

Table 1: Statistics on X-ray Data Collection for the Three Nucleotide Complexes of *E. coli* DHPR

nucleotide	A (Å)	B (Å)	C (Å)	maximum res (Å)	% complete	R_{sym}	% complete to 2.2 Å
NADPH	75.67	81.67	93.94	2.1	93.0	7.7	96.9
NADH	81.17	84.48	91.86	1.9	77.1	7.6	88.1
NHDH	75.56	81.72	93.82	2.0	74.3	6.1	83.0
3-Ac-NADH	81.62	84.56	91.90	2.2	87.3	9.4	87.3

earlier (Scapin et al., 1995). Although crystals were all orthorhombic, space group *I*222, with one molecule per asymmetric unit, crystals obtained using different preparations of enzyme were not isomorphous, with maximum variations of 7% in the unit cell parameters. This nonisomorphism was independent of the nucleotide used for cocrystallization. X-ray diffraction data for all complexes were collected on a Siemens multiwire area detector coupled to a Rigaku RU 200 rotating anode X-ray source operating at 55 V and 80 mA. Data were processed and reduced using the XENGEN software (Howard, 1986), and Table 1 contains statistics for the data collection.

Structure Solution and Refinement. The structure of the *E. coli* DHPR−NADPH binary complex (Scapin et al., 1995), without bound nucleotide or water molecules, was used as a search model to solve the structures of DHPR−NADH, DHPR−NHDH, and DHPR−3-Ac-NADH. Since DHPR−NHDH crystals were completely isomorphous with the DHPR−NADPH complex, molecular replacement was not required to solve the structure. Refinement of this complex was carried out using alternate cycles of computer-based refinement (least-squares positional and temperature factor refinement, as implemented in TNT; Tronrud et al., 1988) and manual rebuilding of the model, using the program TOM (a derivative of FRODO; Jones, 1985) displayed on a Silicon Graphics Iris workstation. Refinement was initiated using data to 2.4 Å, and the bound nucleotide was clearly visible in the initial ($[(F_o - F_c)\phi_c]$) electron density maps and was included in the model. Water molecules were added if (a) there was a 3σ peak in the ($[(F_o - Fc)]\phi_c$) electron density map, (b) there was at least one hydrogen bond with protein atoms or other water molecules, and (c) the modeled water molecules maintained a reasonable temperature factor (<70 Å^2) after refinement. The resolution was slowly increased to include all available data between 20 and 2.2 Å (12 405 reflections with $F > 2\sigma$). Table 2 summarizes the final statistics, after refinement, for the DHPR−NHDH complex.

Crystals of the DHPR−3-Ac-NADH complex were not isomorphous with the DHPR−NADPH crystals. The structure of this complex was solved using molecular replacement (AMORE; Collaborative Computational Project No. 4, 1994; Navaza, 1994) and the structure of the DHPR−NADPH complex, without bound nucleotide or water molecules, as the searching model. A rotation search, carried out between 12 and 4.5 Å, resulted in three equivalent solutions, with correlation coefficients of 12.5, 12.3, and 11.8 (the next solution had a correlation coefficient of 10.7). The three solutions were run through a translation search (between 9 and 4.5 Å), which gave one unambiguous solution, at Eulerian angles of 95.4°, 3.9°, and 81.6° and fractional translations of 0.19, 0.39, and 0.31. The corresponding correlation coefficient and *R*-factor were 32.0 and 49.4, respectively (19.1 and 53.0, respectively, for the next solution). The model obtained by applying the resulting matrix was subjected to 70 cycles of rigid body refinement with X-PLOR (Brunger et al., 1987; Brunger, 1992), using data between 8 and 3 Å, with a 2σ cutoff (5851 reflections, 93% of the possible). The *R*-factor went from 48% to 43.4%. A cycle of simulated annealing (slow cool), as implemented in X-PLOR, run using data between 8 and 2.8 Å, reduced the *R*-factor to 27.7% (the free *R*-factor went from 46.0% to 37.3%). Residues 1−4 and 42−60 were not visible in the resulting map and were initially omitted and then rebuilt into the model. The resolution was increased to 2.4 Å, and at the end of this first cycle, the model contained all but eight residues (residues 1−3 and residues 48−52) and had a conventional *R*-factor of 21.1% (free *R*-factor of 32.8%) for 10 932 reflections with a 2σ cutoff (88% of possible) to 2.4 Å resolution. The RMS deviations from ideality for bond lengths and bond angles were 0.015 Å and 2.07°, respectively. The bound nucleotide was clearly visible in the ($[(F_o - F_c)]\phi_c$) electron density map and was included in the model. Water molecules were added following the same guidelines outlined above. The refinement was continued using TNT, and the resolution was increased to include all available data between 20 and 2.2 Å (13 904 reflections with $F > 2\sigma$, 84% of the possible data). The final model contains 1970 protein atoms, the bound nucleotide, and 69 water molecules. It has a conventional *R*-factor of 19.1%, with good geometry (RMS deviations from ideal bond lengths and bond angles are 0.018 Å and 2.25°, respectively; Table 2).

Table 2: Final Refinement Statistics for the Complexes of *E. coli* DHPR with NHDH, 3-Ac-NADH, and NADH

	complex		
	NHDH	3-Ac-NADH	NADH
res range (Å)	20.0−2.2	20.0−2.2	20.0−2.2
no. of reflections	12405[a]	13904[a]	13953[a]
	12764[b]	14483[b]	14276[b]
(% of possible)	(82[a])	(84[a])	(85[a])
	(85[b])	(87[b])	(87[b])
protein atoms	1980	1970	1974
solvent atoms	81	69	63
ligand atoms	44	44	44
R-factor (%)	18.0[a]	19.1[a]	19.2[a]
	18.5[b]	19.6[b]	19.5[b]
RMS bond length (Å)	0.020	0.018	0.019
RMS bond angle (deg)	1.8	2.3	2.5
⟨*B*⟩ N-ter domain (Å^2)	39.3	36.1	35.8
⟨*B*⟩ C-ter domain (Å^2)	19.5	23.4	22.7
⟨*B*⟩ solvent (Å^2)	40.0	44.3	41.7
⟨*B*⟩ ligand (Å^2)	32.2	33.5	39.4
⟨*B*⟩ loop[c] (Å^2)	72.0	64.7	60.4

[a] A 2σ cutoff has been applied to the reflections throughout the entire refinement. [b] Data in which no cutoff has been applied to the reflections. [c] The loop contains residues 42−58. See text for description.

Crystals of the DHPR−NADH complex were isomorphous with the DHPR−3-Ac-NADH, and the structure of this fourth complex was solved and refined using the DHPR−3-Ac-NADH structure in a manner similar to that previously described for the DHPR−NHDH structure, using TNT as the refinement program. Final statistics for this complex are presented in Table 2.

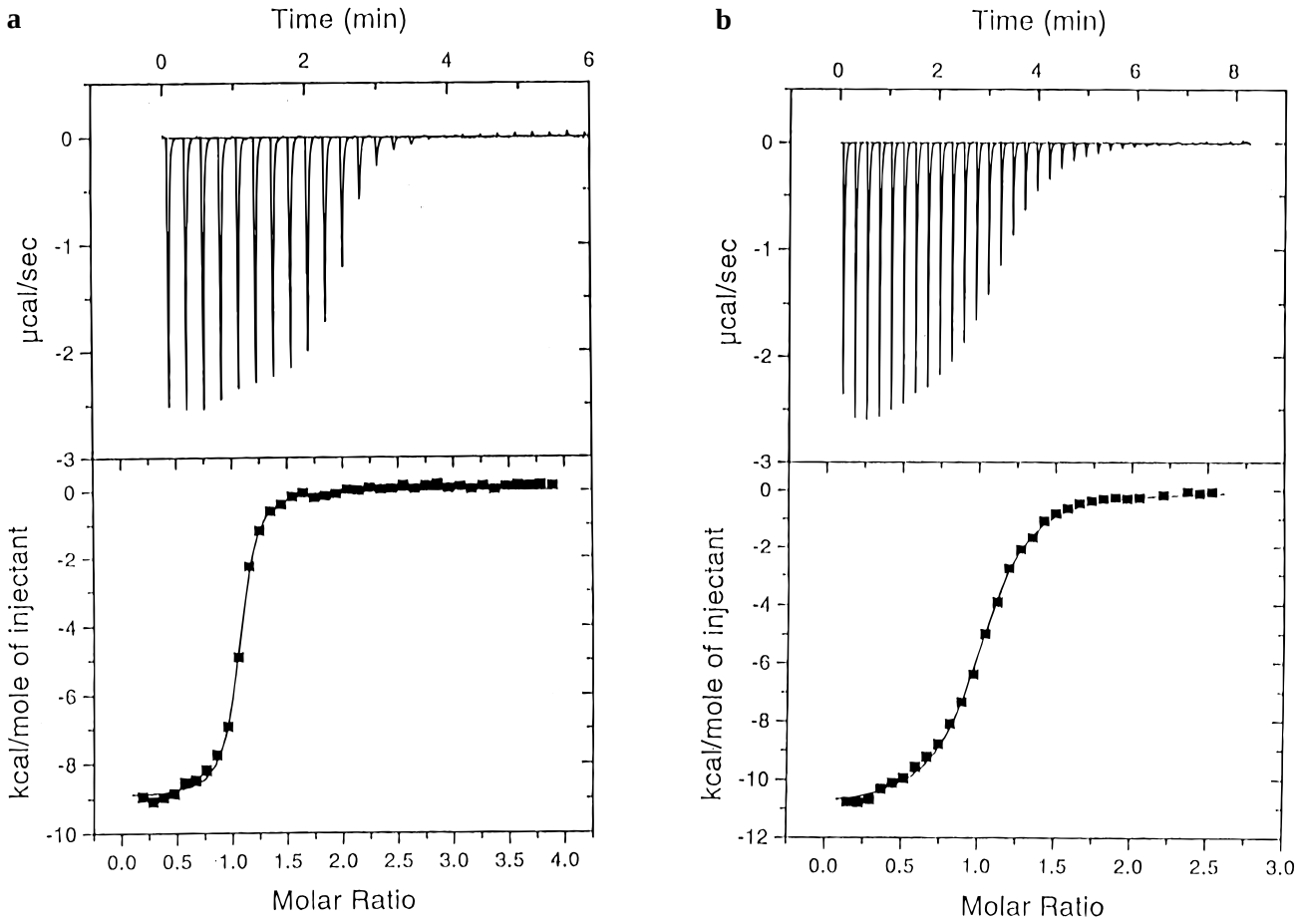

FIGURE 1: Microcalorimetric titration of *E. coli* dihydrodipicolinate reductase with (a) NADH and (b) NADPH. (Top panel) Raw data from the titration. Each peak corresponds to one injection. (Bottom panel) Integrated titration curve fitted by ORIGIN program.

Table 3: Thermodynamic Parameters for Pyridine Nucleotide Binding to *E. coli* DHPR

nucleotide	*n*	K_d (μM)	$\Delta G°$ (kcal/mol)	$\Delta H°$ (kcal/mol)	$\Delta S°$ [cal/(mol·deg)]	$T\Delta S°$ (cal/mol)
NADPH	1.00 ± 0.01	2.12 ± 0.11	−7.81 ± 0.03	−10.98 ± 0.07	−10.5 ± 0.14	−3160 ± 40
3′-NADPH	0.99 ± 0.02	5.05 ± 0.56	−7.29 ± 0.07	−12.18 ± 0.29	−16.3 ± 0.74	−4910 ± 220
TNADPH	1.00 ± 0.01	1.88 ± 0.12	−7.88 ± 0.04	−12.68 ± 0.12	−16.0 ± 0.27	−4820 ± 80
NHDPH	1.02 ± 0.01	3.95 ± 0.22	−7.44 ± 0.03	−8.54 ± 0.08	−3.65 ± 0.16	−1100 ± 50
NADH	1.02 ± 0.01	0.46 ± 0.04	−8.74 ± 0.05	−8.93 ± 0.06	−0.65 ± 0.03	−200 ± 10
TNADH	1.06 ± 0.01	0.28 ± 0.03	−9.02 ± 0.05	−10.54 ± 0.06	−5.05 ± 0.02	−1520 ± 10
3-Ac-NADH	1.01 ± 0.01	0.29 ± 0.05	−9.00 ± 0.10	−8.23 ± 0.08	+2.60 ± 0.06	+780 ± 20
NHDH	1.02 ± 0.01	1.48 ± 0.15	−8.03 ± 0.06	−8.36 ± 0.01	−1.10 ± 0.17	−330 ± 50

RESULTS

Thermodynamic Characterization of DHPR−Nucleotide Complexes. A representative titration experiment is shown in Figure 1. From this binding isotherm it is possible to determine the dissociation constant (K_d), number of binding sites (stoichiometry, *n*), and enthalpic and entropic contributions to the Gibbs free energy of association ($\Delta G° = \Delta H° - T\Delta S°$). This analysis was applied to the investigation of eight DHPR−nucleotide complexes, and the enthalpies and entropies of association for each of the DHPR−nucleotide complexes are listed in Table 3. Comparing the dissociation constants of phosphorylated and nonphosphorylated analogs, it was found that nonphosphorylated nucleotides bind more strongly than phosphorylated nucleotides. Among phosphorylated nucleotides, TNADPH has the highest ($K_d = 1.9$ μM) and 3′-NADPH the lowest ($K_d = 5.0$ μM) affinity for DHPR, while among nonphosphorylated nucleotides, TNADH and 3-Ac-NADH show the highest affinities ($K_d = 0.28$ and 0.29 μM, respectively), while NHDH exhibits the lowest affinity ($K_d = 1.48$ μM). The enthalpies of binding are more favorable for phosphorylated nucleotides compared to their nonphosphorylated counterpart: *ca.* −12.0 kcal mol^{-1} for phosphorylated nucleotides and *ca.* −8.0 kcal mol^{-1} for nonphosphorylated nucleotides. The binding of all nucleotides exhibits negative $\Delta S°$ values, with the exception of 3-Ac-NADH, for which the value is 2.6 cal mol^{-1}, and with phosphorylated nucleotides exhibiting larger negative values than nonphosphorylated nucleotides.

Crystallization Studies: Overall Structure of the Enzyme. *E. coli* DHPR was crystallized in the presence of NADPH, NADH, NHDH, and 3-Ac-NADH, and the structures of all four complexes have been solved and refined to 2.2 Å. Table 2 reports the statistics for the three new complexes determined in this study. The DHPR−NHDH structure contains 272 residues out of 273 (Met1 is missing), the bound nucleotide, and 81 water molecules, respectively. His2, Asp3, Ile6, Arg7, Arg19, Ser42, Ser 47, Glu49, and Gln94

Table 4: RMS Differences of Cα Positions (in Å) between the Four Complexes of *E. coli* DHPR Described in the Text

	NADH		NHDH		3-Ac-NADH	
complex	N-ter	C-ter	N-ter	C-ter	N-ter	C-ter
NADPH	0.38	0.34	0.31	0.19	0.46	0.38
NADH			0.37	0.31	0.22	0.23
NHDH					0.44	0.36

have been modeled as alanines, because of the lack of clear electron density for the side chains. The structures of the DHPR−3-Ac-NADH and DHPR−NADH binary complexes contain residues 4−273, the nucleotide, and 69 and 63 water molecules, respectively. Ser43, Asp48, Glu51, Lys57, Lys70, and Lys187 did not show clear electron density for the side chain, and were modeled as alanines. The amino acids present in all four structures described here have ϕ, ψ angles that fall within the allowed region of low energy of the Ramachandran plot.

The three-dimensional structure of DHPR has been previously described (Scapin et al., 1995). In brief, the enzyme is composed of two domains: a N-terminal domain (residues 2−130 and 240−273) that is composed of seven β-strands and four α-helices which interacts with the bound nucleotide and a C-terminal domain (residues 131−239), composed of four β-strands and two α-helices. The C-terminal domain has been proposed to be the substrate binding region of DHPR (Scapin et al., 1995). *E. coli* DHPR is a tetramer in solution, and although there is only one monomer in the asymmetric unit, the tetramer is generated by a 222 crystallographic symmetry axis. In the tetramer, the four C-terminal domains are involved in extensive subunit−subunit interactions, while the N-terminal domains are more flexible, as shown by the higher temperature factors found for residues in this domain of the enzyme (Table 2).

Analysis of the protein backbone structures of the NADPH, NADH, NHDH, and 3-Ac-NADH complexes shows that the structures of the two domains are very similar, as shown in Table 4. The RMS deviation for Cα positions is generally larger for the N-terminal domain than for the C-terminal domain, in agreement with the higher flexibility found for the nucleotide binding domain. In addition, large differences are observed in the loop composed of residues Ser41 through Thr58 for the four complexes (Figure 2). This loop is characterized by high flexibility, as evidenced by the temperature factors of its atoms (the $\langle B \rangle$ for residues of the loop in the four complexes is $\sim$ 60 Å^2, versus $\sim$36 Å^2 of the whole N-terminal domain; Table 2), and is solvent accessible. Differences are also apparent when comparisons of structures are made between two space groups, and the relative positions of the C- and N-terminal domains are different in the two crystal forms. Overlay of either the N- or the C-terminal regions of the *E. coli* DHPR structure, solved in the two space groups, reveals a rigid body movement of the two domains around two small hinge regions (residues 130−135 and 237−240, data not shown). The effect is due to a rotation of *ca.* 10° of one domain with respect to the other, which brings the dinucleotide binding region and the proposed substrate binding region closer to each other. A more detailed description of this phenomenon and its catalytic implications will be discussed in a subsequent report. This rigid body rotation of the two domains does not alter the structure of the nucleotide binding region (Figure 2), thus allowing a direct comparison to be made between the four complexes, even though they have been obtained from nonisomorphous crystals.

The Dinucleotide Binding Region. Analysis of $((|F_o| - |F_c|)\phi_c)$ difference Fourier maps, calculated for each one of the four complexes, shows the presence of positive electron density across the C-terminal portion of the N-terminal domain which represents the bound nucleotide. In all four complexes, the nucleotide is bound in an extended conformation, with the pyrophosphate moiety located in the crevice formed at the switch point of the β-sheet. Atoms of the nicotinamide mononucleotide moiety are involved in an extensive network of hydrogen bonds with protein atoms, while the adenine portion makes fewer interactions (Figure 3 and Table 5), as evidenced by the weaker electron density for this portion of the nucleotide. In all nonphosphorylated complexes, there is one water molecule tightly bound to the N6 of the adenine. In all complexes, the temperature factors for atoms of the nucleotide increase on going from the nicotinamide to the adenine moiety. All these factors may contribute to reducing the specificity for the adenine moiety. Table 5 summarizes the interactions between nucleotide and protein atoms in the complexes described here. The overall number of interactions is approximately the same for all four nucleotides, but there are some striking differences which contribute to differences in nucleotide binding.

DISCUSSION

The major advantage of titration microcalorimetry is that binding isotherms are determined by the heat of the reaction, allowing the energetics of binding and association constants to be determined. The thermodynamic description of ligand binding with enzymes has been reviewed (Eftink & Biltonen, 1980; Fersht, 1985). Besides contributions from coupled equilibria, such as those involving stoichiometric proton release accompanying ligand binding or changes in the state of aggregation of either component, the observed calorimetric changes result from a combination of (a) complementary

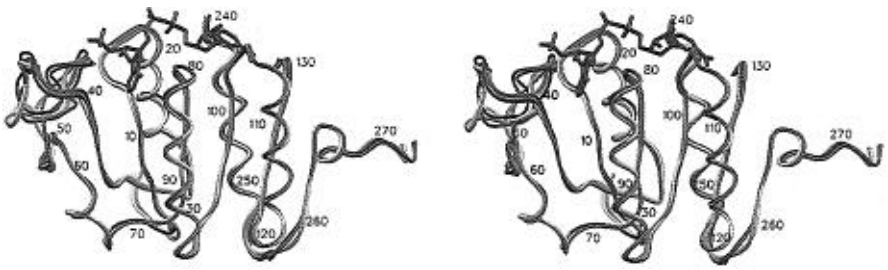

FIGURE 2: Overlay of the Cα backbone of the nucleotide binding domains for the four complexes described in the text. They are color-coded as follows: yellow, DHPR−NADPH; red, DHPR−NADH; light blue, DHPR−NHDH; light green, DHPR−3-Ac-NADH. The same color scheme is used in Figures 5 and 6. This figure and Figures 5 and 6 have been generated with the program SETOR (Evans, 1993).

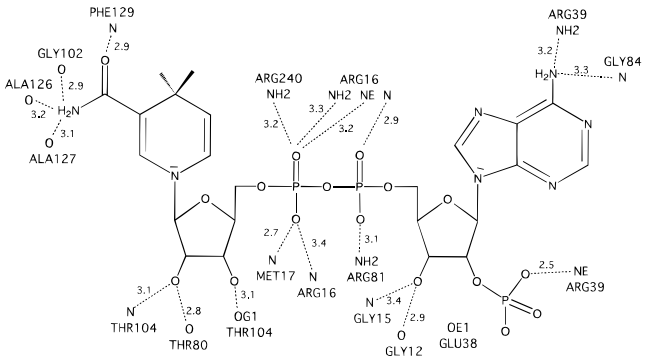

FIGURE 3: Schematic representation of the *E. coli* DHPR nucleotide binding site and the protein−ligand interactions in the DHPR−NADPH complex. Distances are noted in angstroms (see Table 5).

Table 5: Interactions of Nucleotide Atoms with Protein Atoms in the Four *E. coli* DHPR−Nucleotide Complexes Described in the Text[a]

	NADPH	NADH	NHDH	3-Ac-NADH
$\langle B \rangle_{\text{nicotinamide}}$[b]	31.5	31.9	31.7	27.5
$\langle B \rangle_{\text{purine ring}}$	49.4	45.9	44.5	40.6
nicotinamide N7 to				
O Gly102	2.9	3.1	3.1	*c*
O Ala126	3.2	3.3	3.3	*c*
O Ala127	3.1	2.9	3.4	*c*
nicotinamide O7 to				
N Phe129	2.9	2.9	2.7	3.0
ribose O2′ to				
OG1 Thr104	2.8	3.1	2.5	3.3
ribose O3′ to				
O Thr80	2.8	2.8	3.5	3.3
N Thr104	3.1	3.1	3.1	
pyrophosphate to				
N Arg16	2.9, 3.4	2.6, 3.4	3.0	2.8
N Met17	2.7	2.7	2.7	2.5
NE Arg16	3.2	2.6	3.2	
NH2 Arg16	3.3	2.7	3.4	3.0
NH2 Arg81	3.1	2.9, 3.1		3.4
NH2 Arg240	3.2			2.6
Wat				3.3, 3.1
ribose O3′ to				
N Gly15	3.4	3.4	3.3	3.3
O Gly12	2.9	2.7	2.4	2.8
O2 Glu38		3.2	3.0	3.1
ribose O2′ to				
O1 Glu38		2.7	2.4	2.7
O2 Glu38		3.3	3.4	2.7
ribose 2′ phosphate to				
N Arg39	2.5			
adenine (N6 and N3) to				
N Gly84	3.3			3.4
NH2 Arg39	3.2			
Wat		2.6	2.5	2.7

[a] The distances are reported in angstroms. [b] Average temperature factor (in Å^2) for atoms of the nicotinamide/ribose and purine/ribose moieties of bound nucleotides. [c] In this case, the $-NH_2$ group has been replaced with a $-CH_3$, and hydrophobic interactions with the side chain of Phe79 and Phe129 are observed. See text for a more complete discussion.

interactions between the macromolecule and ligand at the binding site through hydrogen bonds, van der Waals forces, or other interactions, (b) changes in the solvation state of the ligand and/or protein, and (c) changes in macromolecular conformations induced by ligand binding. While it is currently not feasible to predict *a priori* the enthalpies and entropies of enzyme−ligand interactions, the magnitude and sign of observed enthalpy or entropy changes are sensitive diagnostic tools for analyzing the interactions that contribute to ligand recognition. Comparisons of the enthalpies and

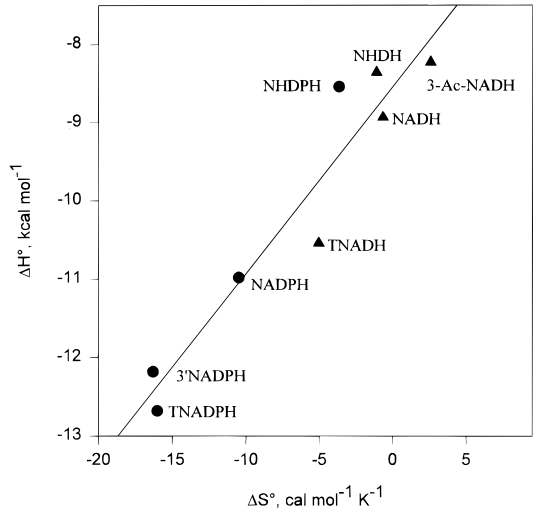

FIGURE 4: Microcalorimetrically determined values of $\Delta H°$ and $\Delta S°$ for the binding of pyridine nucleotides to *E. coli* DHPR. Data for nonphosphorylated nucleotides are shown as filled triangles, and data for phosphorylated nucleotides are shown as filled circles.

entropies of binding from Table 3 for various DHPR−nucleotide complexes dramatically illustrate the interplay that can occur between these parameters during ligand binding. Examination of the values in Table 3 indicates that modest changes in the nucleotide structure (2′-hydroxyl, adenine, and carboxamide regions) can significantly affect the thermodynamic parameters of binding and the affinity of the nucleotide for the protein.

Phosphorylated versus Nonphosphorylated Nucleotide Binary Complexes. The enthalpy changes (Table 3) accompanying enzyme−nucleotide complex formation are exothermic. The $\Delta H°$ values for the binding of nonphosphorylated nucleotides are generally less negative (−8.2 to −10.5 kcal/mol) than are the $\Delta H°$ values for the phosphorylated nucleotides (−10.9 to −12.7 kcal/mol), particularly when phosphorylated and nonphosphorylated pairs are compared. The entropy changes, $\Delta S°$, for the binding of phosphorylated nucleotides are generally large and negative (with the exception of NHDPH), whereas the $\Delta S°$ for the nonphosphorylated nucleotides are near zero or slightly positive. The relation between the thermodynamic parameters for nucleotide binding can be illustrated by the entropy−enthalpy compensation plot (Lumry & Rajender, 1970; Figure 4). Enthalpy−entropy compensation is a common phenonmenon in biopolymer processes occurring in aqueous solvent (Lumry & Rajender, 1970), with the result that $\Delta G°$ is less temperature-dependent than either $\Delta H°$ or $\Delta S°$. For DHPR a linear relationship between the determined values of $\Delta H°$ and $\Delta S°$ is observed, with the phosphorylated and nonphophorylated nucleotides clustering into two regions. Similar enthalpy−entropy compensation has been observed both as a function of ligand structure and also as a function of protein structure, using mutagenesis approaches (Kelly & O'Connell, 1993; Brummell et al., 1993; Ito et al., 1993). We will focus this discussion of comparisons between phosphorylated and nonphosphorylated nucleotides on the physiologically relevant reductants, NADPH and NADH.

Structural analysis of the NADPH and NADH complexes shows that there is a significant difference in the protein structure which is dependent on the 2′-adenosyl ribose substituent of the bound nucleotide. While in both com-

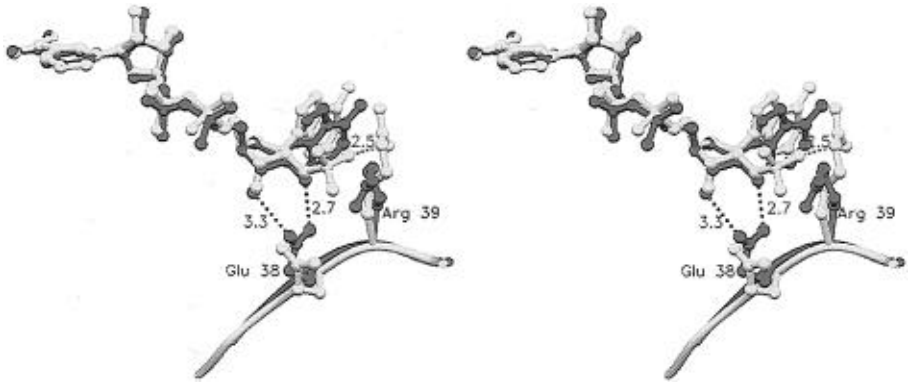

FIGURE 5: Superposition of the bound nucleotides, and the positions of the side chains of Arg39 and Glu38, observed in the DHPR−NADPH (yellow) and DHPR−NADH (red) complexes.

plexes the nicotinamide moiety of NADPH and NADH is superimposable (Figure 5), in the DHPR−NADH complex the adenine ring has moved deeper into the binding site compared to the DHPR−NADPH complex, accompanied by a structural rearrangement of the region spanning residues 37−40, especially the side chains of Glu38 and Arg39. The single electrostatic interaction observed between Arg39 and the 2′-phosphate, an interaction observed in many other NADPH-dependent proteins (Bystroff et al., 1990; Scrutton et al., 1990; Sem & Kasper, 1993), has been replaced in the DHPR−NADH complex by two new hydrogen bonds between the carboxyl side chain of Glu38 and the 2′- and 3′-ribose hydroxyls (Figure 5, red). This network of hydrogen bonds is similar to that observed between the conserved acidic residue and the adenosyl ribose in other NADH-dependent enzymes (Baker et al., 1992a,b).

Hydrogen-bonding interactions generally contribute about 2 kcal/mol to the enthalpy term for each hydrogen bond, with an accompanying decrease in the entropy (Eftink & Biltonen, 1980). Electrostatic interactions between charged groups, on the other hand, are characterized by higher enthalpy terms (Eftink & Biltonen, 1980), and this may explain the larger value of $\Delta H°$ observed for NADPH, compared to NADH, binding. The large negative entropy term observed for NADPH binding suggests that there may be a high degree of complementarity between NADPH, and other 2′-phosphonucleotides, and the enzyme which restricts the motion of side chains in their binary complexes. Results from the crystallographic analysis suggest that the mobility of the side chain of Arg39 is restricted after binding. Comparisons of the position and average temperature factor for the side chain atoms of Arg39 in the four complexes show that while, in the DHPR−NADPH complex, this side chain is well defined with an $\langle B \rangle$ of 59 Å^2, in the three complexes with nonphosphorylated nucleotides, the side chain of Arg39 occupies slightly different positions in each complex, and the $\langle B \rangle$ for its side chain atoms is ∼78 Å^2, indicating a higher degree of flexibility. The ordering of an arginine side chain upon binding of NADPH has recently been reported for 6-phosphogluconate dehydrogenase (Adams et al., 1994). Another contribution to the more negative entropic term for NADPH binding may be attributed to the loss of rotational freedom of the 2′-phosphate group.

NADH and NHDH. NHDH binds to *E. coli* DHPR with a dissociation constant of 1.48 μM, compared to the corresponding value for NADH of 0.46 μM. This 3-fold difference results from the substitution of the exocyclic amino group of the adenine ring with the keto group of the hypoxanthine ring. This substitution would be expected to alter the pattern of hydrogen bond formation, since the hydrogen bond donating amino group has been replaced with a hydrogen bond accepting keto group. In DHPR−nucleotide complexes, the adenine ring is less rigidly bound than the nicotinamide ring, and thus its contribution to the binding affinity may be expected to be modest. Comparison of the structures of the NADH and NHDH complexes shows that, in fact, there are only minor differences in the positioning of the purine rings but that the side chain of Arg39 assumes different conformations in the two complexes. In both complexes the side chain atoms of Arg39 show an $\langle B \rangle$ of 78 Å^2, indicative of a high degree of flexibility. In the NADH complex, Arg39 is loosely interacting (3.2 Å) with a water molecule, while this interaction is not observed in the NHDH complex, which may account for the slightly lower $\Delta H°$ value observed for DHPR−NHDH complex formation. The small difference in entropy (−1.1 vs −0.65 for NADH) may be due to the slightly more favorable interaction between the alkyl side chain of Arg39 and the hypoxanthine ring of NHDH.

TNADH and NADH. The replacement of the oxygen atom in the carboxamido side chain with sulfur enhances the enthalpy of binding of the nonphosphorylated and phosphorylated nucleotide for DHPR by *ca.* 1.5 kcal/mol, although the more negative $\Delta H°$ is partially compensated by the smaller increase in the $\Delta S°$ values. In the NADH complex, the oxygen atom of the carboxamide interacts with the main chain nitrogen of Phe129 (Table 5), but it is also within van der Waals contact distance from the hydrophobic side chain of Phe243. Sulfur is less electronegative and a weaker hydrogen-bonding partner than oxygen, but is larger and more polarizable than oxygen, and may interact strongly enough with the hydrophobic environment, particularly Phe243, to account for the ∼1.5 kcal/mol of additional enthalpy. This favorable interaction between the sulfur and the side chain of Phe243 may be similar to Van der Waals interactions observed in the structure of the 3-Ac-NADH−DHPR complex (see below) and may also be reflected in the modest increase in $\Delta S°$ as a result of the more restricted motion of the Phe243 side chain.

3-Acetyl-NADH/NADH. 3-Ac-NADH is almost two times more tightly bound than NADH. While the $\Delta H°$ for the formation of the two complexes is almost identical (Table 3), the binding of 3-Ac-NADH is entropically more favorable (+2.6 versus −0.65 cal mol^{-1} deg^{-1}). Analysis of the

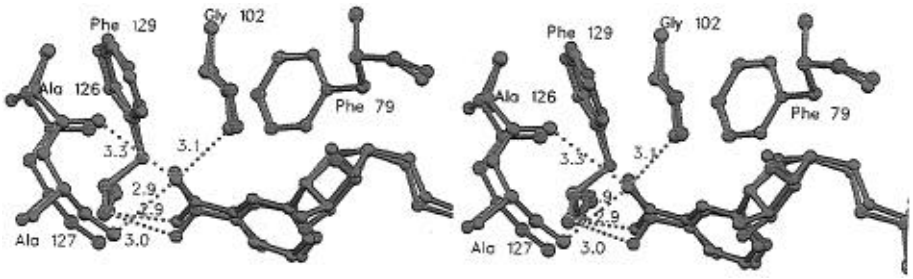

FIGURE 6: Superposition of the nicotinamide (or 3-acetylpyridine) rings of the bound nucleotides in the DHPR−NADH (red) and DHPR−3-Ac-NADH (light green) complexes.

conformation of the bound nucleotide in the two binary structures (Figure 6) shows that the three hydrogen bonds made by the NH_2 group of the carboxamido group of NADH (to the backbone carbonyls of Gly102, Ala126, and Ala127) are replaced by van der Waal interactions of the methyl group of the acetyl side chain with the aromatic rings of the side chains of Phe79 and Phe129. This causes the acetyl side chain to twist out of coplanarity with the nicotinamide ring. The presence of these hydrophobic interactions must compensate for the loss of the hydrogen bonds, since the enthalpy of binding is not significantly different for 3-Ac-NADH and NADH. The unusual positive value of $\Delta S°$ may be caused by a decreased conformational restriction of the main chain segment containing Ala126 and Ala127 in the DHPR−3-Ac-NADH complex. In support of this proposal, the temperature factors for main chain atoms of Ala126 and Ala127 exhibit an average increase of 9 and 3 Å^2, respectively, in the 3-Ac-NADH complex compared to the NADH complex.

Conclusions. Our original supposition that DHPR represented an appropriate subject for the detailed thermodynamic and structural investigation of pyridine nucleotide binding has been validated in the present study. While the absolute values of the thermodynamic dissociation constants are due to a large number of individual interactions between DHPR and the nucleotide (Figure 4), comparisons between structural homologs can reveal specific interactions which can be interpreted. In particular, the comparison of NADH and NADPH binding reveals an intriguing change in thermodynamic driving force. In the case of NADPH, the binding is enthalpically very favorable but is entropically disfavored by almost 3 kcal/mol at 25 °C. The dominant enthalpic contribution is the formation of a strong electrostatic interaction between the 2′-phosphate monoester and the side chain of Arg39. This interaction also restricts the rotation of the 2′-phosphate and the allowed conformations of the Arg39 side chain, which may account for the very unfavorable entropic effect. In contrast, NADH binding is enthalpically less favored by 2 kcal/mol but has a minimal unfavorable entropic component. The single strong electrostatic interaction observed between DHPR and NADPH is replaced by two hydrogen bonds between the adenosyl ribose hydroxyl groups of NADH and Glu38. The side chain of Arg39 assumes a different conformation in the DHPR−NADH complex and is more flexible, as evidenced by its higher thermal factor, $\langle B \rangle$. These conclusions about the thermodynamic contributions to nucleotide binding are generally extendable to other phosphorylated and nonphosphorylated nucleotide substrate pairs studied.

The comparison between the binding of NADH and 3-Ac-NADH is also noteworthy in this regard. The binding of 3-Ac-NADH to DHPR is stronger than NADH binding by a factor of 2, and this is predominantly due to a uniquely favorable entropy effect accompanying binding. The RMS differences of Cα positions of protein atoms are slight in the DHPR−NADH and DHPR−3-Ac-NADH complexes, as are the conformations of the two bound nucleotides. The loss of hydrogen bonding between the carboxamido nitrogen and the backbone carbonyl oxygen atoms of Gly102, Ala126, and Ala127 is likely to be the source of the 0.7 kcal/mol loss of enthalpy for 3-Ac-NADH binding, compared to NADH binding. The presence of hydrophobic side chains adjacent to the carboxamido binding site permits the acetyl group of 3-Ac-NADH to twist out of coplanarity with the pyridine ring and insert between the phenyl rings of Phe79 and Phe129. The very favorable entropic effect observed for 3-Ac-NADH binding may be the result of the loss of the conformational restriction of the main chain in which the two hydrogen-bonding alanine residues are located.

REFERENCES

Adams, M. J., Ellis, G. H., Gover, S., Naylor, C. E., & Phillips, C. (1994) *Structure 2*, 651−668.

Baker, P. J., Britton, K. L., Rice, D. W., Rob, A., & Stillman, T. J. (1992a) *J. Mol. Biol. 228*, 662−671.

Baker, P. J., Britton, K. L., Engel, P. C., Farrants, G. W., Lilley, K. S., Rice, D. W., & Stillman, T. J. (1992b) *Proteins 12*, 75−86.

Bradford, M. (1976) *Anal. Biochem. 72*, 248.

Breslauer, K. J., Remeta, D. P., Chou, W.-Y., Ferrante, R., Curry, J., Zaunczkowski, D., Snyder, J. G., & Marky, L. A. (1987) *Proc. Natl. Acad. Sci. U.S.A. 84*, 8922−8926.

Brummell, D. A., Sharma, V. P., Anand, N. N., Bilous, D., Dubuc, G., Michniewicz, J., MacKenzie, C. R., Sadowska, J., Sigurskjold, B. W., Sinnott, B., Young, N. M., Bundle, D. R., & Narang, S. A. (1993) *Biochemistry 32*, 1180−1187.

Brunger, A. T. (1992) *X-PLOR version 3 manual: a system for crystallography and NMR*, Yale University, New Haven, CT.

Brunger, A. T., Kuriyan, J., & Karplus, M. (1987) *Science 235*, 458−460.

Bystroff, C., Oatley, S. J., & Kraut, J. (1990) *Biochemistry 29*, 3263−3277.

Cirillo, J. D., Weisbrod, T. R., Banerjee, A., Bloom, B. R., & Jacobs, W. R., Jr. (1994) *J. Bacteriol. 176*, 4424−4429.

Collaborative Computational Project No. 4 (1994) The CCP4 suite: programs for protein crystallography, *Acta Crystallogr. D50*, 760−763.

DeMoss, R. D., Gunsalus, I. C., & Bard, R. C. (1953) *J. Bacteriol. 66*, 10−16.

Eftink, M., & Biltonen, R. (1980) in *Biological Microcalorimetry* (Beezer, A. E., Ed.) pp 343−412, Academic Press, New York.

Evans, S. V. (1993) *J. Mol. Graphics 11*, 134−138.

Fersht, A. (1985) in *Enzyme Structure and Mechanism*, pp 294−310, W. H. Freeman, New York.

Howard, A. J. (1986) *A guide to data reduction for the Nicolet Imaging Proportional Counter: the XENGEN system*, Protein Engineering Department, Genex Corp., Gaithersburg, MD.

Ito, W., Iba, Y., & Kurosawa, Y. (1993) *J. Biol. Chem. 268*, 16639−16647.
John, J., Crennel, S. J., Hough, D. W., Danson, M. J., & Taylor, G. L. (1994) *Structure 2*, 385−393.
Jones, T. A. (1985) *Methods Enzymol. 115*, 157−171.
Karplus, P. A., & Schulz, G. E. (1989) *J. Mol. Biol. 210*, 163−180.
Kelly, R. F., & O'Connell, M. P. (1993) *Biochemistry 32*, 6828−6835.
Lumry, R., & Rajender, S. (1970) *Biopolymers 9*, 1125−1227.
Male, K. B., & Storey, K. B. (1982) *Int. J. Biochem. 14*, 1083−1089.
Navaza, J. (1994) *Acta Crystallogr. D50*, 157−163.
Quigley, F., Brinkmann, H., Martin, W. F., & Cerff, R. (1989) *J. Mol. Evol. 29*, 412−421.
Reddy, S. G., Sacchettini, J. C., & Blanchard, J. S. (1995) *Biochemistry 34*, 3492−3501.
Scapin, G., Blanchard, J. S., & Sacchettini, J. C. (1995) *Biochemistry 34*, 3502−3512.
Scrutton, N. S., Berry, A., & Perham, R. N. (1990) *Nature 343*, 38−43.
Sem, D. S., & Kasper, C. B. (1993) *Biochemistry 32*, 11548−11558.
Tronrud, D. E., Ten Eyck, L. F., & Mathews, B. W. (1988) *Acta Crystallogr., A43*, 489−501.
Wiseman, T., Williston, S., Brandts, J. F., & Lin, L.-N. (1989) *Anal. Biochem. 179*, 131.

BI9615809